1 Theory of Linear Response in a Nutshell

This section summarizes some important derivations from [Vonsovskii and Katsnel'son, 1989] and [Giuliani and Vignale, 2005] that are crutial for further calculations.

Classically Consider an electron system subject to small external perturbation $V_{\text{ext}}(\mathbf{r}, t)$. By definition of the *inverse dielectric function* the total potential $V(\mathbf{r}, t)$ is given by

$$V(\mathbf{r}, t) = \int \mathrm{d}^3 r' \int_{-\infty}^{t} \mathrm{d}t' \; \varepsilon^{-1}(\mathbf{r}, \mathbf{r}', t - t') V_{\text{ext}}(\mathbf{r}', t') \; . \tag{1}$$

The upper bound of the integral over t' is t in place of ∞ due to causality: the "effect" cannot precede the "cause". This is equivalent to saying that $\varepsilon^{-1}(\mathbf{r}, \mathbf{r}', \tau) = 0$ whenever $\tau < 0$. The Fourier transform of $\varepsilon^{-1}(\mathbf{r}, \mathbf{r}', \tau)$ is

$$\varepsilon^{-1}(\mathbf{r}, \mathbf{r}', \omega) = \int_{0}^{\infty} \mathrm{d}\tau \; e^{i\omega\tau} \, \varepsilon^{-1}(\mathbf{r}, \mathbf{r}', \tau) \; . \tag{2}$$

Applying Titchmarsh's theorem to ε^{-1}, we get that $\varepsilon^{-1}(\mathbf{r}, \mathbf{r}', \omega)$ is the limit $\eta \to 0+$ of $\varepsilon^{-1}(\mathbf{r}, \mathbf{r}', \omega + i\eta)$ which is holomorphic in the upper complex plane. Taking Fourier transform of eq. (1), we obtain[1]

$$V(\mathbf{r}, \omega) = \int \mathrm{d}^3 r' \; \varepsilon^{-1}(\mathbf{r}, \mathbf{r}', \omega) V_{\text{ext}}(\mathbf{r}', \omega) \; . \tag{3}$$

Eqs. (2) and (3) may equivalently be formulated as

$$\begin{aligned} V_{\text{ext}}(\mathbf{r}, \omega) &= \int \mathrm{d}^3 r' \varepsilon(\mathbf{r}, \mathbf{r}', \omega) V(\mathbf{r}') \; , \text{ where} \\ \varepsilon(\mathbf{r}, \mathbf{r}', \omega) &= \lim_{\eta \to 0+} \varepsilon(\mathbf{r}, \mathbf{r}', \omega + i\eta) = \lim_{\eta \to 0+} \int_{0}^{\infty} \mathrm{d}\tau \; e^{i(\omega + i\eta)\tau} \, \varepsilon(\mathbf{r}, \mathbf{r}', \tau) \; . \end{aligned} \tag{4}$$

[1]

$$\begin{aligned} V(\mathbf{r}, \omega) &= \int_{-\infty}^{\infty} \mathrm{d}t \; e^{i\omega t} \, V(\mathbf{r}, t) \\ &= \int \mathrm{d}^3 r' \int_{-\infty}^{\infty} \mathrm{d}t \int_{-\infty}^{t} \mathrm{d}t' \; e^{i\omega t} \, \varepsilon^{-1}(\mathbf{r}, \mathbf{r}', t - t') V_{\text{ext}}(\mathbf{r}', t') \\ &= \int \mathrm{d}^3 r' \int_{-\infty}^{\infty} \frac{\mathrm{d}\omega'}{2\pi} \int_{-\infty}^{\infty} \mathrm{d}t \int_{-\infty}^{t} \mathrm{d}t' \; e^{i\omega t} e^{-i\omega' t'} \varepsilon^{-1}(\mathbf{r}, \mathbf{r}', t - t') V_{\text{ext}}(\mathbf{r}', \omega') \\ &= \int \mathrm{d}^3 r' \int_{-\infty}^{\infty} \frac{\mathrm{d}\omega'}{2\pi} V_{\text{ext}}(\mathbf{r}', \omega') \int_{-\infty}^{\infty} \mathrm{d}t \int_{-\infty}^{t} \mathrm{d}t' \; e^{i(\omega - \omega')t} e^{i\omega'(t - t')} \, \varepsilon^{-1}(\mathbf{r}, \mathbf{r}', t - t') \\ &= \int \mathrm{d}^3 r' \int_{-\infty}^{\infty} \frac{\mathrm{d}\omega'}{2\pi} \; V_{\text{ext}}(\mathbf{r}', \omega') \int_{-\infty}^{\infty} \mathrm{d}t \, e^{i(\omega - \omega')t} \int_{\infty}^{0} (-\mathrm{d}\tau) \; e^{i\omega'\tau} \, \varepsilon^{-1}(\mathbf{r}, \mathbf{r}', \tau) \\ &= \int \mathrm{d}^3 r' \int_{-\infty}^{\infty} \mathrm{d}\omega' \, \varepsilon^{-1}(\mathbf{r}, \mathbf{r}', \omega') V_{\text{ext}}(\mathbf{r}', \omega') \cdot \frac{1}{2\pi} \int_{-\infty}^{\infty} \mathrm{d}t \; e^{i(\omega - \omega')t} \\ &= \int \mathrm{d}^3 r' \; \varepsilon^{-1}(\mathbf{r}, \mathbf{r}', \omega) V_{\text{ext}}(\mathbf{r}', \omega) \; . \end{aligned}$$

Quantum Mechanically Now consider a system of non-interacting electrons described in a single-particle approximation by a Hamiltonian $\hat{H}_0$. Let E_i denote single-particle energy levels with corresponding eigenstates $|i\rangle$. One-particle density matrix is then

$$\hat{\rho}_0 = \sum_i n_i \, |i\rangle\langle i| \; , \tag{5}$$

where n_i denotes the occupational number at energy E_i which, in equilibrium, is given by the Fermi-Dirac distribution. Electron density operator is $\hat{N}(\mathbf{r}) = |\mathbf{r}\rangle\langle\mathbf{r}|$. Equation of motion reads

$$i\hbar \frac{\mathrm{d}\hat{\rho}_0}{\mathrm{d}t} = [\hat{H}_0, \hat{\rho}_0] = 0 \; .$$

Within RPA (Random Phase Approximation) we are interested in the reponse of the system to the perturbation of the form $\hat{V}e^{-i(\omega+i\eta)t}$.[2] In the first order approximation, $\hat{\rho} = \hat{\rho}_0 + \hat{\rho}' + \mathcal{O}(\hat{V}^2)$, where $\hat{\rho}_0$ is defined by eq. (5) and $\hat{\rho}' \propto \hat{V}$. We thus have

$$\left.\begin{aligned} i\hbar\frac{\mathrm{d}\hat{\rho}}{\mathrm{d}t} &= i\hbar\frac{\mathrm{d}\hat{\rho}_0}{\mathrm{d}t} + i\hbar\frac{\mathrm{d}\hat{\rho}'}{\mathrm{d}t} \\ [\hat{H},\hat{\rho}] &= [\hat{H}_0,\hat{\rho}_0] + [\hat{H}_0,\hat{\rho}'] + [\hat{V},\hat{\rho}_0]e^{-i(\omega+i\eta)t} + \mathcal{O}(\hat{V}^2) \end{aligned}\right\} \implies i\hbar\frac{\mathrm{d}\hat{\rho}'}{\mathrm{d}t} = [\hat{H}_0,\hat{\rho}'] + [\hat{V},\hat{\rho}_0]e^{-i(\omega+i\eta)t} \; . \tag{6}$$

Using an ansatz $\hat{\rho}' = \widetilde{G}\hat{V}e^{-i(\omega+i\eta)t}$, where $\widetilde{G}$ is some time-independent operator, we obtain[3]

$$\begin{aligned} \langle i|\widetilde{G}\hat{V}|j\rangle &= \frac{n_i - n_j}{E_i - E_j - \hbar(\omega + i\eta)}\langle i|\hat{V}|j\rangle \\ &\equiv \langle i|\hat{G}|j\rangle \, \langle i|\hat{V}|j\rangle \; , \end{aligned}$$

where we have defined a new operator $\hat{G}$ by

$$\langle i|\hat{G}|j\rangle = \frac{n_i - n_j}{E_i - E_j - \hbar(\omega + i\eta)} \; . \tag{7}$$

We can now calculate the induced electron density $\delta\hat{N}(t)$:

$$\begin{aligned} \langle \mathbf{r}|\delta\hat{N}(t)|\mathbf{r}\rangle &= \mathrm{Tr}(\hat{N}(\mathbf{r})\hat{\rho}) - \mathrm{Tr}(\hat{N}(\mathbf{r})\hat{\rho}_0) = \mathrm{Tr}(\hat{N}(\mathbf{r})\hat{\rho}') \\ &= \sum_{i,j}\langle j|\mathbf{r}\rangle\langle\mathbf{r}|i\rangle\langle i|\widetilde{G}\hat{V}|j\rangle e^{-i(\omega+i\eta)t} \\ &= \sum_{i,j}\langle i|\hat{G}|j\rangle\langle j|\mathbf{r}\rangle\langle\mathbf{r}|i\rangle\langle i|\hat{V}|j\rangle e^{-i(\omega+i\eta)t} \; . \end{aligned} \tag{8}$$

[2] Notice the appearance of η. It may be viewed either mathematically, as trick to be able to use eq. 4, or physically, as an adiabatic turning on of the potential. For further discussion of the significance of this factor, see [Nussenzveig, 1972]

[3] Calculating matrix elements:

$$\begin{aligned} \langle i|i\hbar\frac{\mathrm{d}\hat{\rho}'}{\mathrm{d}t}|j\rangle &= \hbar(\omega + i\eta)\langle i|\hat{\rho}'|j\rangle \; , \\ \langle i|[\hat{H}_0,\hat{\rho}']|j\rangle &= (E_i - E_j)\langle i|\hat{\rho}'|j\rangle \; , \\ \langle i|[\hat{V},\hat{\rho}_0]|j\rangle &= (n_j - n_i)\langle i|\hat{V}|j\rangle \; . \end{aligned}$$

Eq. (6) now reads

$$\langle i|\hat{\rho}'|j\rangle = \frac{(n_i - n_j)\, e^{-i\omega t + \eta t}}{E_i - E_j - \hbar(\omega + i\eta)}\langle i|\hat{V}|j\rangle \; .$$

The total potential $\hat{V}$ is the sum of external potential $\hat{V}_{\text{ext}}$ and the potential induced by the variation of the charge density, i.e.

$$\langle \mathbf{r}|\hat{V}_{\text{tot}}(t)|\mathbf{r}\rangle = \langle \mathbf{r}|\hat{V}_{\text{ext}}(t)|\mathbf{r}\rangle + \int \mathrm{d}^3 r' \; \langle \mathbf{r}|\hat{V}_{\text{Coulomb}}|\mathbf{r}'\rangle\langle \mathbf{r}'|\delta\hat{N}(t)|\mathbf{r}'\rangle \; , \tag{9}$$

where $\hat{V}_{\text{Coulomb}}$ is the Coulomb interaction potential. We have also used the fact that $\hat{V}$ is diagonal in position representation. Using eq. (8) we get[4]

$$\begin{aligned}
\langle \mathbf{r}|\hat{V}_{\text{ext}}(t)|\mathbf{r}\rangle &= \int \mathrm{d}^3 r' \; \langle \mathbf{r}|\hat{\varepsilon}(t)|\mathbf{r}'\rangle\langle \mathbf{r}'|\hat{V}|\mathbf{r}'\rangle \; , \text{ where} \\
\langle \mathbf{r}|\hat{\varepsilon}(\tau)|\mathbf{r}'\rangle &= \left(\langle \mathbf{r}|\mathbf{r}'\rangle - \sum_{i,j} \langle i|\hat{G}|j\rangle \int \mathrm{d}^3 r'' \; \frac{e^2}{\|\mathbf{r}-\mathbf{r}''\|} \, \langle j|\mathbf{r}''\rangle\langle \mathbf{r}''|i\rangle\langle i|\mathbf{r}'\rangle\langle \mathbf{r}'|j\rangle \right) e^{-i(\omega+i\eta)\tau} \; .
\end{aligned}$$

Using Titchmarsh's theorem once again, we obtain

$$\begin{aligned}
\langle \mathbf{r}|\hat{V}_{\text{ext}}(\omega)|\mathbf{r}\rangle &= \int \mathrm{d}^3 r' \; \langle \mathbf{r}|\hat{\varepsilon}(\omega)|\mathbf{r}'\rangle\langle \mathbf{r}'|\hat{V}|\mathbf{r}'\rangle \; , \text{ where} \\
\langle \mathbf{r}|\hat{\varepsilon}(\omega)|\mathbf{r}'\rangle &= \lim_{\eta\to 0+} \langle \mathbf{r}|\hat{\varepsilon}(\omega+i\eta)|\mathbf{r}'\rangle = \lim_{\eta\to 0+} \int_0^\infty \mathrm{d}\tau \; e^{i(\omega+i\eta)\tau} \, \langle \mathbf{r}|\varepsilon(\tau)|\mathbf{r}'\rangle \\
&= \langle \mathbf{r}|\mathbf{r}'\rangle - \lim_{\eta\to 0+} \sum_{i,j} \langle i|\hat{G}|j\rangle \int \mathrm{d}^3 r'' \; \frac{e^2}{\|\mathbf{r}-\mathbf{r}''\|} \, \langle j|\mathbf{r}''\rangle\langle \mathbf{r}''|i\rangle\langle i|\mathbf{r}'\rangle\langle \mathbf{r}'|j\rangle \\
&= \langle \mathbf{r}|\mathbf{r}'\rangle - \int \mathrm{d}^3 r'' \; \langle \mathbf{r}|\hat{V}_{\text{Coulomb}}|\mathbf{r}''\rangle\langle \mathbf{r}''|\hat{\chi}(\omega)|\mathbf{r}'\rangle \; , \\
\langle \mathbf{r}''|\hat{\chi}(\omega)|\mathbf{r}'\rangle &= \lim_{\eta\to 0+} \sum_{i,j} \langle i|\hat{G}|j\rangle\langle j|\mathbf{r}''\rangle\langle \mathbf{r}''|i\rangle\langle i|\mathbf{r}'\rangle\langle \mathbf{r}'|j\rangle \; , \\
\langle \mathbf{r}|\hat{V}_{\text{Coulomb}}|\mathbf{r}''\rangle &= \frac{e^2}{\|\mathbf{r}-\mathbf{r}''\|} \; ,
\end{aligned} \tag{10}$$

which is the exact equivalent of eq. (4) in the classical description. $\hat{\chi}$ is called the *polarizability matrix*.

[4] At point $\mathbf{r}$ we have

$$\begin{aligned}
\langle \mathbf{r}|\hat{V}_{\text{ext}}(t)|\mathbf{r}\rangle &= \langle \mathbf{r}|\hat{V}_{\text{tot}}(t)|\mathbf{r}\rangle - \int \mathrm{d}^3 r' \; \frac{e^2}{\|\mathbf{r}-\mathbf{r}'\|} \, \langle \mathbf{r}'|\delta\hat{N}(t)|\mathbf{r}'\rangle \\
&\overset{(8)}{=} \langle \mathbf{r}|\hat{V}|\mathbf{r}\rangle e^{-i(\omega+i\eta)t} - \int \mathrm{d}^3 r' \; \frac{e^2}{\|\mathbf{r}-\mathbf{r}'\|} \sum_{i,j} \langle i|\hat{G}|j\rangle \, e^{-i(\omega+i\eta)t} \, \langle j|\mathbf{r}'\rangle\langle \mathbf{r}'|i\rangle\langle i|\hat{V}|j\rangle \\
&= \left(\langle \mathbf{r}|\hat{V}|\mathbf{r}\rangle - \sum_{i,j} \langle i|\hat{G}|j\rangle \int \mathrm{d}^3 r' \int \mathrm{d}^3 r'' \int \mathrm{d}^3 r''' \; \frac{e^2}{\|\mathbf{r}-\mathbf{r}'\|} \, \langle j|\mathbf{r}'\rangle\langle \mathbf{r}'|i\rangle\langle i|\mathbf{r}''\rangle\langle \mathbf{r}'''|j\rangle\langle \mathbf{r}''|\hat{V}|\mathbf{r}'''\rangle \right) e^{-i(\omega+i\eta)t} \\
&= \left(\langle \mathbf{r}|\hat{V}|\mathbf{r}\rangle - \sum_{i,j} \langle i|\hat{G}|j\rangle \int \mathrm{d}^3 r' \int \mathrm{d}^3 r'' \; \frac{e^2}{\|\mathbf{r}-\mathbf{r}'\|} \, \langle j|\mathbf{r}'\rangle\langle \mathbf{r}'|i\rangle\langle i|\mathbf{r}''\rangle\langle \mathbf{r}''|j\rangle\langle \mathbf{r}''|\hat{V}|\mathbf{r}''\rangle \right) e^{-i(\omega+i\eta)t} \; .
\end{aligned}$$

2 Application

We now apply the results of sec. 1 to a finite 2D lattice described in the tight binding approximation. We do the calculation in *atomic basis*, i.e. the basis of local site wave functions $|a\rangle$ ($a \in \{0, N-1\}$, where N is the number of sites). The following assumptions are made:

- $\langle a|b\rangle = \delta_{a,b}$,
- atomic basis is complete, i.e. $\sum_a |a\rangle\langle a| = \hat{\mathbb{1}}$,
- $|a\rangle$'s are localized around the corresponding sites, i.e. $\langle \mathbf{r}|a\rangle \approx \delta(\mathbf{r} - \mathbf{r_a})$, where $\mathbf{r_a}$ is the position of a'th site. This is the key to making a step from analytical formulas to numerical calculations.

These assumptions essentially mean that the step from position representation to atomic basis is performed by $|\mathbf{r}\rangle \to |a\rangle$, $\mathbf{r} \to \mathbf{r_a}$ and $\int \mathrm{d}^3 r \to \sum_a$. Another important step is to replace $\hat{G}$ by $2\hat{G}$. Now i and j indices also run from 0 to $N-1$. Eq. (10) now reads[5]

$$\begin{aligned}
\langle a|\hat{V}_{\text{ext}}(\omega)|a\rangle &= \sum_b \langle a|\hat{\varepsilon}(\omega)|b\rangle\langle b|\hat{V}|b\rangle \ , \text{ where} \\
\langle a|\hat{\varepsilon}(\omega)|b\rangle &= \langle a|b\rangle - \sum_c \langle a|\hat{V}_{\text{Coulomb}}|c\rangle\langle c|\hat{\chi}(\omega)|b\rangle \ , \\
\langle a|\hat{\chi}(\omega)|b\rangle &= 2 \cdot \lim_{\eta\to 0+} \sum_{i,j} \langle i|\hat{G}|j\rangle\langle j|a\rangle\langle a|i\rangle\langle i|b\rangle\langle b|j\rangle \ , \\
\langle a|\hat{V}_{\text{Coulomb}}|b\rangle &= \begin{cases} \dfrac{1}{4\pi\epsilon_0}\dfrac{e}{\|\mathbf{r_a} - \mathbf{r_b}\|} & \text{, if } a \neq b, \\ V_0 & \text{, if } a = b, \end{cases}
\end{aligned} \tag{11}$$

The trick that allows the calculations of $\hat{\chi}(\omega)$ in a reasonable time is to rewrite it in terms of matrices:

$$\begin{aligned}
\langle a|\hat{\chi}(\omega)|b\rangle &= \overbrace{A(a,b)}^{\text{row vector}} \underbrace{\hat{G}}_{\text{square matrix}} \overbrace{A(a,b)^\dagger}^{\text{column vector}} = \overbrace{\Big(\underbrace{\hat{G}^{\mathrm{T}} A(a,b)^{\mathrm{T}}}_{\texttt{GEMV}}\Big)^{\mathrm{T}} A(a,b)^\dagger}^{\texttt{DOT}} \ , \text{ where} \\
G_{i,j} &= \langle i|\hat{G}|j\rangle \overset{(7)}{=} \frac{n_i - n_j}{E_i - E_j - \hbar(\omega + i\eta)} \quad \text{with } \eta \text{ small, and} \\
A(a,b)_i &= \langle a|i\rangle\langle i|b\rangle = \langle a|i\rangle\langle b|i\rangle^* \ .
\end{aligned} \tag{12}$$

The second form of $\langle a|\hat{\chi}(\omega)|b\rangle$ with a lot of transposes may seem strange, but it is of utmost importance. It allows us to calculate matrix elements of $\hat{\chi}(\omega)$ using just two `BLAS` operations: matrix-vector product (`GEMV`) and dot-product (`DOT`). It is now straightforward to write a highly parallel implementation of eq. (12) and it will not be discussed here any further.

With eqs. (11) and (12) implemented, we can obtain $\hat{\varepsilon}(\omega)$ for any system, given its tight-binding Hamiltonian $\hat{H}$ and sites positions $\big\{\mathbf{r_a} \big| a \in \{0, \ldots, N-1\}\big\}$.

[5] Eq. (10) was written in Gauss system. For the calculations it is, however, easier to use electron-volts. We thus replace e^2 by $\frac{e}{4\pi\epsilon_0}$. We also introduce the *self-interaction potential* V_0 to prevent degeneracies in $\langle a|\hat{V}_{\text{Coulomb}}|a\rangle$.

3 Experiments

Let's now apply the aquired tools to examine plasmonic properties of some systems. For this we need a way of visualising the results. The most common way to measure plasmonic properties is through EELS (*E*lectron *E*nergy *L*oss *S*pectroscopy) experiments. We will not discuss these experiments in detail. A good explanation in-depth explanation may be found in [Egerton, 2009]. EELS works great for systems exhibiting translational symmetry. For such systems $\varepsilon(\mathbf{r}, \mathbf{r}', \omega) = \varepsilon(\mathbf{r} - \mathbf{r}', \omega)$. This function is then Fourier transformed into $\varepsilon(\mathbf{q}, \omega)$, and $-\operatorname{Im}[\varepsilon(\mathbf{q}, \omega)^{-1}]$ is the *loss function*, a measurable quantity. Our focus, however, relies on fractals, i.e. systems that don't have translational symmetry. $\varepsilon(\mathbf{q}, \omega)$ is thus not well defined — another approach is needed.

[Wang Weihua et al., 2015] provides an example. It goes as follows. Consider the classical definition of a plasmon: $\varepsilon(\omega) = 0$. In reality, there is also loss due to the parameter $\eta \neq 0$ in eq. (11). We then decompose the dielectric function

$$\hat{\varepsilon}(\omega) = \sum_n \epsilon_n(\omega)\, |\phi_n(\omega)\rangle\langle\phi_n(\omega)|$$

and identify plasmons by

$$\hat{\varepsilon}(\omega)|\phi_n(\omega)\rangle = \epsilon_n(\omega)|\phi_n(\omega)\rangle \ , \text{ with } \epsilon_n(\omega) \in \mathbb{C} \setminus \mathbb{R}, \text{ i.e. purely imaginary.} \tag{13}$$

As noted in [Andersen et al., 2012], "when the imaginary part of eigenvalue $\epsilon_n(\omega)$ does not vary too much around the plasmon frequency ω'", condition (13) is equivalent to the condition that

$$-\operatorname{Im}[\epsilon_n^{-1}(\omega)] \text{ has a local maximum at } \omega' \ . \tag{14}$$

In [Wang Weihua et al., 2015] the *loss function* is then defined as $-\operatorname{Im}[\epsilon_{n(\omega)}^{-1}(\omega)]$, where $n(\omega)$ is the index of the eigenvalue with the highest $-\operatorname{Im}[\epsilon_j^{-1}(\omega)]$. This provides us a "real space analogue" of $-\operatorname{Im}[\varepsilon^{-1}(\mathbf{q}, \omega)]$. Fig. 1 gives an example of how loss spectrum may look like. Huge number of sharp peaks looks like noise at first glance. A closer look shows that this is

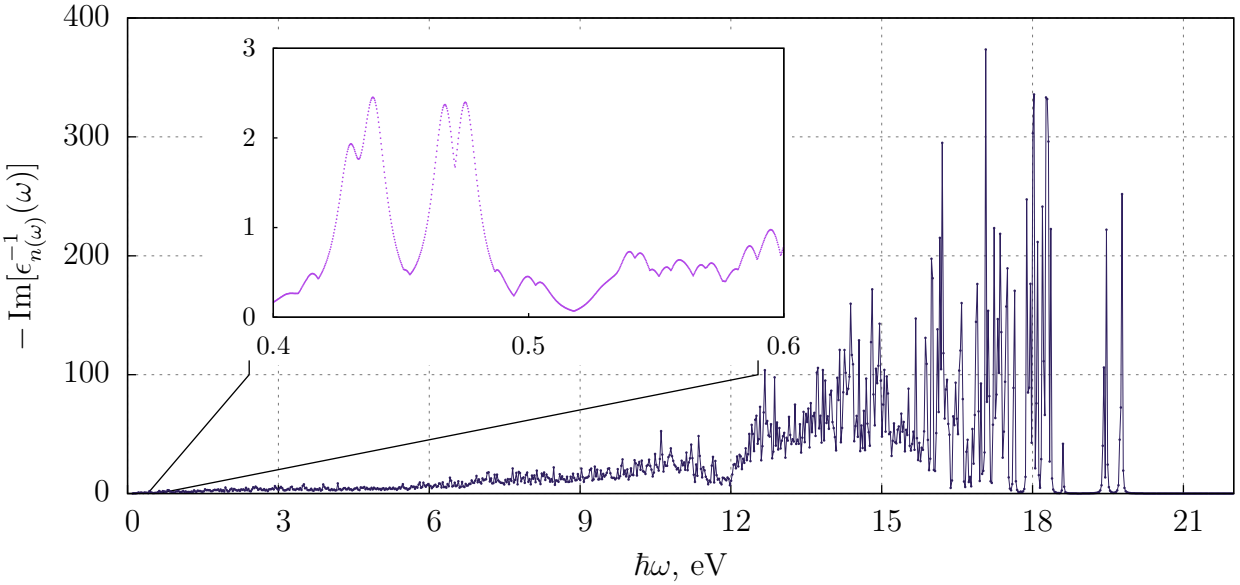

Figure 1: Loss function spectrum for the third iteration Sierpinski carpet. The spectrum is highly fluctuating. This makes one wonder whether this spectrum represents actual physical results.

not the case. All in all, this makes one doubt the validity of the definition of the loss function

used in [Wang Weihua et al., 2015]. Furthermore, there are no formal arguments provided that support such a definition. Finally, for each $(\omega, n(\omega))$ pair, $\mathrm{Re}[\langle \mathbf{r}|\phi_{n(\omega)}(\omega)\rangle]$ gives a good insight in how the plasmon modes "look like". There are, however, no known experiments where measurements of $\mathrm{Re}[\langle \mathbf{r}|\phi_{n(\omega)}(\omega)\rangle]$ were performed.

Another approach is to try to express some measurable quantity using $\varepsilon(\omega)$. An, obviously, measurable quantity would be the electron charge distribution. From eq. (10), we get[6]

$$\langle \mathbf{r}|\hat{V}|\mathbf{r}\rangle = \int \mathrm{d}^3 r' \, \langle \mathbf{r}|\hat{\varepsilon}^{-1}(\omega)|\mathbf{r}'\rangle \langle \mathbf{r}'|\hat{V}_{\mathrm{ext}}(\omega)|\mathbf{r}'\rangle \; .$$

We can now insert this result into eq. (9) to obtain

$$\langle \mathbf{r}|\delta\hat{N}(\omega)|\mathbf{r}\rangle = \int \mathrm{d}^3 r'' \, \langle \mathbf{r}|\hat{V}^{-1}_{\mathrm{Coulomb}}|\mathbf{r}''\rangle \cdot \left(\int \mathrm{d}^3 r' \, \langle \mathbf{r}''|\hat{\varepsilon}^{-1}(\omega)|\mathbf{r}'\rangle \langle \mathbf{r}'|\hat{V}_{\mathrm{ext}}(\omega)|\mathbf{r}'\rangle - \langle \mathbf{r}''|\hat{V}_{\mathrm{ext}}(\omega)|\mathbf{r}''\rangle \right) \; .$$

3.1 Third iteration Sierpinski carpet

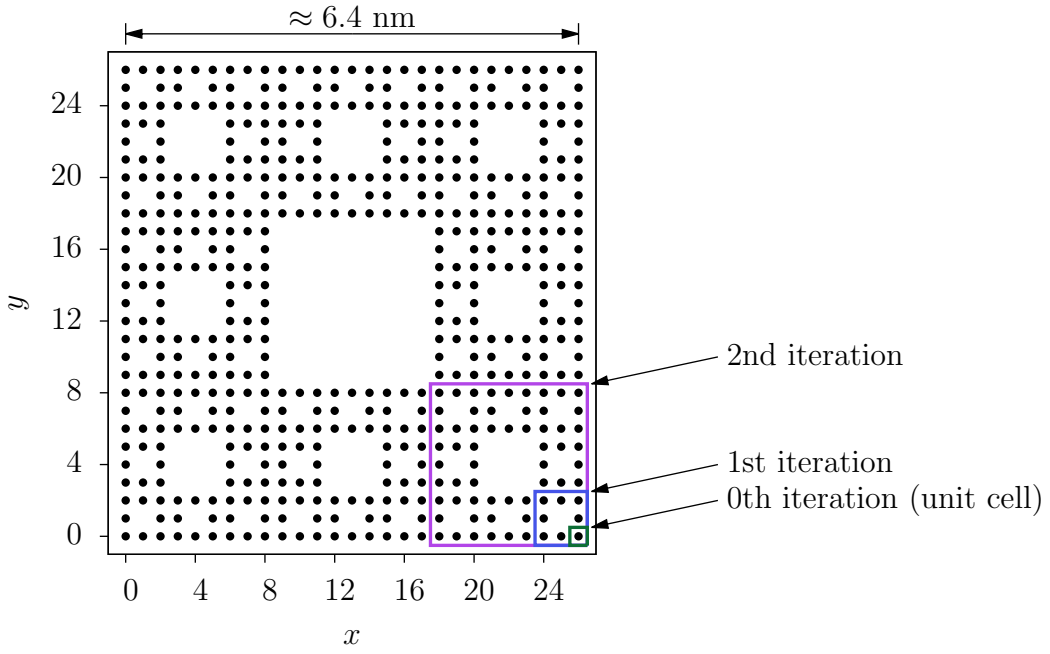

Figure 2: Third iteration Sierpinski carpet. x and y coordinates are given in terms of lattice constant. Width of the sample is $3^3 = 27$ unit cells. In this case we chose the lattice constant of graphene $a \approx 0.246$ nm, which results in the total width of about six and a half nanometers.

6

$$\langle \mathbf{r}|\hat{V}_{\mathrm{ext}}(\omega)|\mathbf{r}\rangle = \int \mathrm{d}^3 r' \, \langle \mathbf{r}|\hat{\varepsilon}(\omega)|\mathbf{r}'\rangle \langle \mathbf{r}'|\hat{V}|\mathbf{r}'\rangle$$

$$\int \mathrm{d}^3 r \, \langle \mathbf{r}''|\hat{\varepsilon}^{-1}(\omega)|\mathbf{r}\rangle \langle \mathbf{r}|\hat{V}_{\mathrm{ext}}(\omega)|\mathbf{r}\rangle = \int \mathrm{d}^3 r' \int \mathrm{d}^3 r \, \langle \mathbf{r}''|\hat{\varepsilon}^{-1}(\omega)|\mathbf{r}\rangle \langle \mathbf{r}|\hat{\varepsilon}(\omega)|\mathbf{r}'\rangle \langle \mathbf{r}'|\hat{V}|\mathbf{r}'\rangle$$

$$\int \mathrm{d}^3 r \, \langle \mathbf{r}''|\hat{\varepsilon}^{-1}(\omega)|\mathbf{r}\rangle \langle \mathbf{r}|\hat{V}_{\mathrm{ext}}(\omega)|\mathbf{r}\rangle = \int \mathrm{d}^3 r' \, \langle \mathbf{r}''|\mathbf{r}'\rangle \langle \mathbf{r}'|\hat{V}|\mathbf{r}'\rangle$$

$$\int \mathrm{d}^3 r \, \langle \mathbf{r}''|\hat{\varepsilon}^{-1}(\omega)|\mathbf{r}\rangle \langle \mathbf{r}|\hat{V}_{\mathrm{ext}}(\omega)|\mathbf{r}\rangle = \langle \mathbf{r}''|\hat{V}|\mathbf{r}''\rangle$$

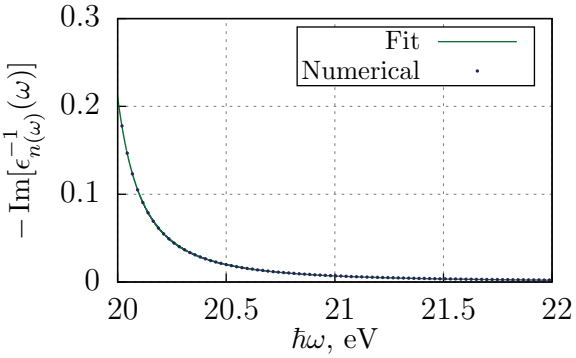

Figure 4: This plot shows asymptotic behavior of the loss function at high frequencies. "Numerical" denotes the results of the precise numerical calculation. "Fit" is obtained by fitting $a/((b-\omega)^2+c^2)$ (i.e. eq. (15)) to the results of numerical calculations. LSA (Least Square Approximation) gives the following values for the parameters: $a = 1.031 \times 10^{-2}$, $b = 19.779$, $c = 8 \times 10^{-4}$.

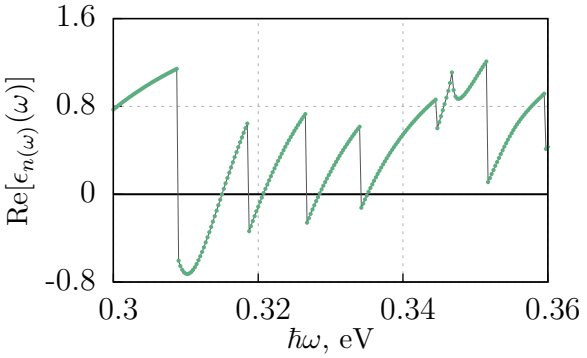

Figure 5: Behavior of $\mathrm{Re}[\epsilon_{n(\omega)}(\omega)]$ is shown. A really narrow interval of frequencies is chosen for clarity. Roots where the sign of $\mathrm{Re}[\epsilon_{n(\omega)}(\omega)]$ changes from -1 to $+1$ are well defined. We identify them with plasmon frequencies.

We start by examining a small system — third iteration Siepinski carpet. The sample is shown in fig. 2. Using TIPSI Python package we can construct a tight-binding Hamiltonian for the problem. Hopping value of 2.8 eV is used. As we need eigenenergies and eigenstates anyway to make use of eq. (11), we can have a look at the density of states (fig. 3). Although the number of points is quite small (512 atomic sites), we can still extract some information. For example, all possible energies lie within the $(-9.5\text{ eV}, 9.5\text{ eV})$ range. Hence, $E_i - E_j < 19$ eV for any i, j. $G_{i,j}$ has $(E_i - E_j - \hbar(\omega + i\eta))$ in the denominator, thus for ω's greater than ≈ 20 eV, $-\mathrm{Im}[\epsilon^{-1}_{n(\omega)}(\omega)]$ will asymptotically approach zero — no need to search for plasmons there.

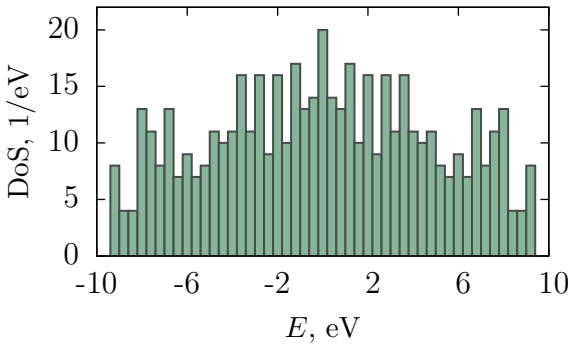

Figure 3: Density of states for the 3rd iteration SC. Due to the small size of the system, we can't say much about the distribution of energy eigenvalues. Except that it's highly fluctuating — as one would expect for a fractal system.

To calculate the dielectric function, we need to choose a couple more parameters of the system. For now, we, again, follow [Wang Weihua et al., 2015] and let the temperature T of the system be 300 K, chemical potential $\mu = 0.4$ eV, self-interaction coulomb potential $V_0 = 15.78$ eV, and the "inverse relaxation time" $\hbar\eta = 0.006$ eV.

Having chosen all configuration parameters we calculate $\hat{\varepsilon}(\omega)$ for frequencies up to ≈ 22 eV. The two extra eV allow us to look at asymptotic behavior at high frequencies. Let's ignore for a minute the fact that $\hat{\epsilon}(\omega)$ is a matrix. Using eq. (11) we can approximate the dielectric function by

$$\epsilon(\omega) \approx 1 - \frac{A}{B - \omega + i \cdot C} ,$$

and the loss function becomes[7]

$$-\operatorname{Im}[\epsilon(\omega)^{-1}] \approx \frac{a}{(b-\omega)^2 + c^2} \ , \text{ where } a = AC, \ \ b = B - A, \ \ c = C \ . \tag{15}$$

Fig. 4 shows how good this approximation actually is. This verifies our hypothesis that $\max_{i,j}|E_i - E_j|$ is a reasonable upper bound for plasmon frequencies.

Spectrum for the full range of frequencies is shown on fig. 1. With our definition of a plasmon, high number of sharp peaks means that there are plenty of plasmons. It is interesting to compare the classical definition of plasmon to the condition that loss function has a local maximum. For this we focus on the low-energy part of the spectrum in fig. 1 as low-energy plasmon modes are easier to excite experimentally (**TODO:** this is my intuition, but is it actually true?).

Classically, we defined plasmon frequencies as roots of $\operatorname{Re}[\epsilon_{n(\omega)}(\omega)]$. However, if we plot $\operatorname{Re}[\epsilon_{n(\omega)}(\omega)]$ vs. ω (see fig. 5), we notice that roots where the sign changes from $+1$ to -1 are not well defined. These are just discontinuities. Hence, extend the definition of plasmon frequencies to account for that:

$$\operatorname{Re}[\epsilon_{n(\omega')}(\omega')] = 0 \ \text{ and } \lim_{\omega \to \omega' +} \operatorname{sign}\big(\operatorname{Re}[\epsilon_{n(\omega)}(\omega)]\big) - \lim_{\omega \to \omega' -} \operatorname{sign}\big(\operatorname{Re}[\epsilon_{n(\omega)}(\omega)]\big) = 2 \ .$$

With this improved definition we can now check whether conditions (13) and (14) are indeed equivalent. For this we plot the loss function spectrum and mark the points where the real part of the dielectric function crosses zero from below. Fig. 6 shows such a spectrum.

We see that "classical" plasmon frequencies are indeed located near maxima of the loss function. As noted by [Andersen et al., 2012], it's not important that the peaks do not coincide with roots of $\operatorname{Re}[\epsilon_{n(\omega)}(\omega)]$ as long as the eigenstates $|\phi_{n(\omega)}(\omega)\rangle$ do not vary much. We can verify this by calculating $|\langle\phi_{n(\omega_i)}(\omega_i)|\phi_{n(\omega_{i+1})}(\omega_{i+1})\rangle|$, where ω_i's denote frequencies for which we have calculated $\hat{\varepsilon}$. It turns out that except for the points where we "step over" from one peak to another, $|\langle\phi_{n(\omega_i)}(\omega_i)|\phi_{n(\omega_{i+1})}(\omega_{i+1})\rangle| \approx 1$ with variations of order 1%.

This means that to know how plasmon eigenstates look like, we do not even need to know the precise location of the maximum of $-\operatorname{Im}[\epsilon^{-1}_{n(\omega)}(\omega)]$ or the zero of $\operatorname{Re}[\epsilon_{n(\omega)}(\omega)]$. Knowledge that we are on a particular peak suffices. As an example, fig. 7 and 8 show $\operatorname{Re}[\langle\mathbf{r}|\phi_{n(\omega)}(\omega)\rangle]$ for two high peaks at around 0.467 eV and 0.475 eV (see fig. 6).

Localised plasmon eigenmodes are easier to control and thus are highly valuable for experimental applications. We use IPR (*I*nverse *P*articipation *R*atio) as a measure of localisation. In our case IPR for an eigenstate $|\phi\rangle$ is defined as

$$\operatorname{IPR}|\phi\rangle = \sum_a |\langle a|\phi\rangle|^4 \ . \tag{16}$$

The higher the IPR of a state, the more localised it is. For example, a completely localised state $|a\rangle$ has an IPR of 1, while a spread out state like $\frac{1}{\sqrt{N}}\sum_a |a\rangle$ has an IPR of order $\mathcal{O}(N^{-2})$.

---

[7]

$$\begin{aligned}
-\operatorname{Im}[\epsilon(\omega)^{-1}] &= -\operatorname{Im}\left[\left(1 - \frac{A}{B - \omega + i\cdot C}\right)^{-1}\right] = -\operatorname{Im}\left[\frac{B - \omega + i\cdot C}{B - A - \omega + i\cdot C}\right] \\
&= -\operatorname{Im}\left[\frac{(B - \omega + i\cdot C)(B - A - \omega - i\cdot C)}{(B - A - \omega)^2 + C^2}\right] = -\frac{-C(B-\omega) + C(B - A - \omega)}{(B - A - \omega)^2 + C^2} \\
&= \frac{CA}{(B - A - \omega)^2 + C^2} \ .
\end{aligned}$$

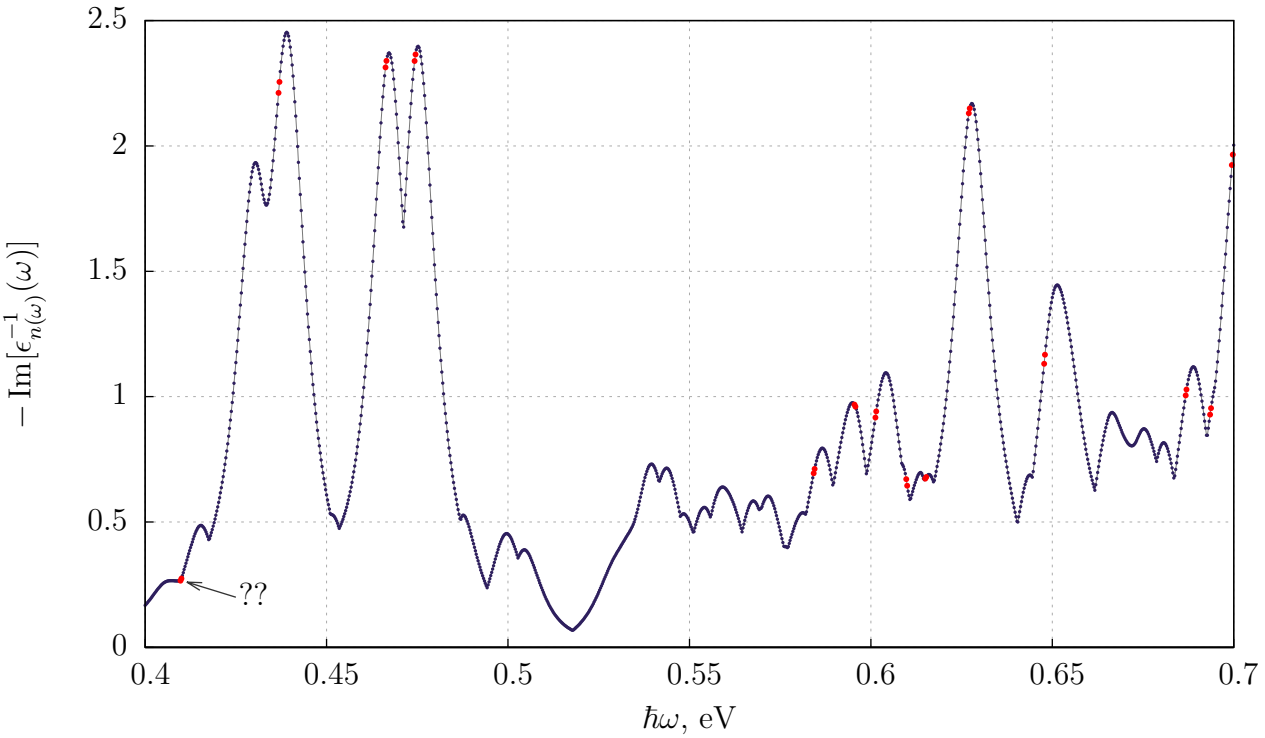

Figure 6: Loss function spectrum with "classical" plasmons marked in red. Most plasmons appear near maxima of the loss function — in accordance with [Andersen et al., 2012]. At least one plasmon, however, appears at frequency where the derivative of the loss function exhibits a discontinuity. This plasmon is marked with an arrow in the plot. A closer look at the real part of the dielectric function shows that $\mathrm{Re}[\epsilon_{n(\omega)}(\omega)]$ *changes its sign in a discontinuous step. We thus consider this point a false positive and not a plasmon.*

References

[Andersen et al., 2012] Andersen, K., Jacobsen, K. W., and Thygesen, K. S. (2012). Spatially resolved quantum plasmon modes in metallic nano-films from first-principles. *Physical Review B*, 86(24):245129.

[Egerton, 2009] Egerton, R. (2009). Electron energy-loss spectroscopy in the TEM. *Reports on Progress in Physics*, 72(1):016502.

[Giuliani and Vignale, 2005] Giuliani, G. and Vignale, G. (2005). *Quantum Theory of the Electron Liquid*. Masters Series in Physics and Astronomy. Cambridge University Press.

[Nussenzveig, 1972] Nussenzveig, H. (1972). *Causality and Dispersion Relations*. Mathematics in Science and Engineering. Elsevier Science.

[Vonsovskii and Katsnel'son, 1989] Vonsovskii, S. V. and Katsnel'son, M. I. (1989). *Quantum solid-state physics*, volume 73. Springer Verlag.

[Wang Weihua et al., 2015] Wang Weihua, Christensen Thomas, Jauho Antti-Pekka, Thygesen Kristian S., Wubs Martijn, and Mortensen N. Asger (2015). Plasmonic eigenmodes in individual and bow-tie graphene nanotriangles. *Scientific Reports*, 5:9535.

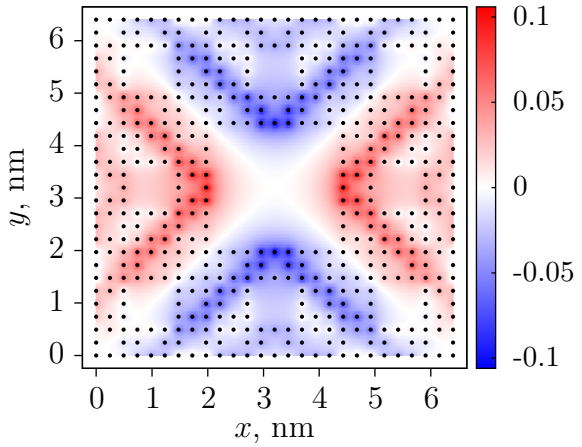

Figure 7: Plasmon eigenmode at frequency corresponding to $\hbar\omega = 0.46625\ eV$

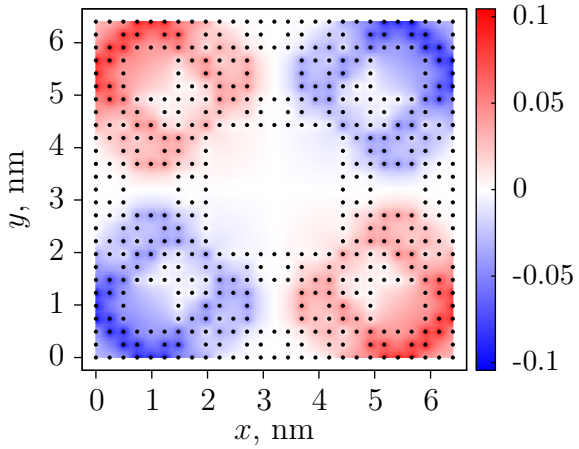

Figure 8: Plasmon eigenmode at frequency corresponding to $\hbar\omega = 0.47425\ eV$

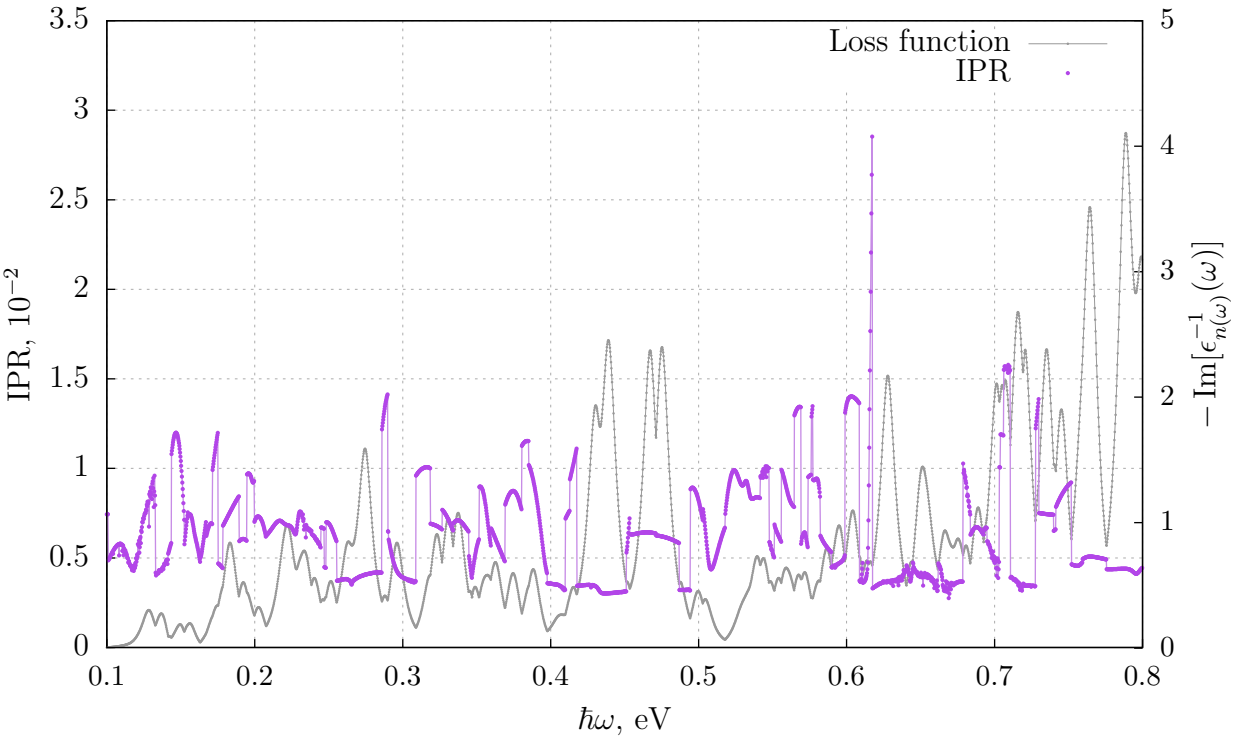

Figure 9